I_2 imidazoline receptor modulation protects aged SAMP8 mice against cognitive decline by suppressing the calcineurin pathway

Foteini Vasilopoulou[1], Christian Griñán-Ferré[1], Sergio Rodríguez-Arévalo[2], Andrea Bagán[2], Sònia Abás[2], Carmen Escolano[2], and Mercè Pallàs[1]*

[1]Pharmacology Section, Department of Pharmacology, Toxicology and Medicinal Chemistry, Faculty of Pharmacy and Food Sciences, and Institute of Neurociencies, University of Barcelona, Av. Joan XXIII, 27-31, E-08028 Barcelona, Spain.

[2]Laboratory of Medicinal Chemistry (Associated Unit to CSIC), Department of Pharmacology, Toxicology and Medicinal Chemistry, Faculty of Pharmacy and Food Sciences, and Institute of Biomedicine (IBUB), University of Barcelona, Av. Joan XXIII, 27-31, E-08028 Barcelona, Spain.

*Corresponding author:

Mercè Pallàs, PhD

pallas@ub.edu

Pharmacology Section, Department of Pharmacology, Toxicology and Medicinal Chemistry, Faculty of Pharmacy and Food Sciences, and Institut de Neurociències, University of Barcelona, Av. Joan XXIII, 27-31, E-08028 Barcelona, Spain.

Keywords: I_2 Imidazoline receptors, aging, behavior, neuroinflammation, NFAT, neuroprotection, Alzheimer's disease.

Abbreviations

AD, Alzheimer's disease; Aldh2, aldehyde dehydrogenase 2; APP, amyloid precursor protein; BAD, BCL-2 associated agonist of cell death; Bdnf, brain-derived neurotrophic factor; CaMKII, calcium calmodulin kinase II; CaN, calcineurin; CDK5, cyclin dependent kinase; cDNA, complementary DNA; CREB, cAMP response element-binding; Ct, cycle threshold; Cxcl-10, C-X-C motif chemokine ligand 10; (EAAT)2, cxcitatory aminoacid transporter 2; ERK, cxtracellular signal–regulated Kinase; GAPDH, glyceraldehyde-3-phosphate dehydrogenase; GFAP, glial fibrillary acid protein; GSK3β, glycogen synthase kinase 3β; H_2O_2, hydrogen peroxide; Hmox 1, hemoxygenase 1; I_2-IR, imidazoline 2 receptors; Ide, insulin degrading enzyme; Ifnγ, interferon-γ; iNOS, inducible nitric oxide synthase; LTD, long-term depression; LTP, long-term potentiation; MAO, Monoamineoxidase; mRNA, messenger RNA; Nep, neprilysin; NFATc1, nuclear factor of activated T-cells Cytoplasmic 1; NMDA, N-Methyl-D-aspartate; NMDAR, N-Methyl-D-aspartate receptor; NORT, novel object recognition test; Nrf1, nuclear factor-erythroid2-related factor 1; OFT, open field test; OS, oxidative stress; p-Tau, hyperphosphorylated Tau; PD, Parkinson's disease; PKA, protein kinase A; PP2B, phosphatase 2B; PVDF, polyvinylidene difluoride; ROS, reactive oxygen species; qPCR, real-time quantitative PCR; RT-PCR, reverse transcription-polymerase chain reaction; SAMP8, senescence-accelerated mouse prone 8; sAPPα, soluble APP α; sAPPβ, soluble APP β; SDS-PAGE, sodium dodecyl sulphate-polyacrylamide gel electrophoresis; SEM, standard error of the mean; TBS-T, tween 20 TBS; TBS, tris-buffered saline; TN, novel object, new location; Tnf-α, tumor necrosis factor alpha; TO, old object, old location; TrkB, tropomyosin-related kinase B; WB, western blotting; ΔΔCt, cycle threshold method.

Abstract

Brain aging and dementia are current problems that must be solved. The levels of imidazoline 2 receptors (I_2-IRs) are increased in the brain in Alzheimer's disease (AD) and other neurodegenerative diseases. We tested the action of the specific and selective I_2-IR ligand B06 in a mouse model of accelerated aging and AD, the senescence-accelerated mouse prone 8 (SAMP8) model. Oral administration of B06 for four weeks improved SAMP8 mouse behavior and cognition and reduced AD hallmarks, oxidative stress, and apoptotic and neuroinflammation markers. Likewise, B06 regulated glial excitatory amino acid transporter 2 and N-methyl-D aspartate 2A and 2B receptor subunit protein levels. Calcineurin (CaN) is a phosphatase that controls the phosphorylation levels of cAMP response element-binding (CREB), apoptotic mediator BCL-2-associated agonist of cell death (BAD) and GSK3β, among other molecules. Interestingly, B06 was able to reduce the levels of the CaN active form (CaN A). Likewise, CREB phosphorylation, BAD gene expression, and other factors were modified after B06 treatment. Moreover, phosphorylation of a target of CaN, nuclear factor of activated T-cells, cytoplasmic 1 ($NFAT_{C1}$), was increased in B06-treated mice, impeding the transcription of genes related to neuroinflammation and neural plasticity. In summary, this I_2 imidazoline ligand can exert its beneficial effects on age-related conditions by modulating CaN pathway action and affecting several molecular pathways, playing a neuroprotective role in SAMP8 mice.

1. Introduction

Aging has become a problem worldwide, since older people are more prone to develop chronic and degenerative diseases. At the brain level, aging affects several molecular pathways that predispose patients to neurodegeneration, causing dementia, cognitive impairment and loss of quality of life. Among dementias, the most prevalent is Alzheimer's disease (AD) (GBD 2016 Neurology Collaborators, 2019). AD has aroused considerable interest because of its strong influence on quality of life among elderly individuals and because of the limited drugs available to combat cognitive loss and neuropsychiatric symptoms.

β-Amyloid deposition in senile plaques and tau hyperphosphorylation forming neurofibrillary tangles are specific hallmarks of AD (Serrano-Pozo et al. 2011). However, there are no successful pharmacological treatments that modify the progression of AD, given that acetylcholinesterase inhibitors and memantine fail to stop the progression of dementia (Cummings et al. 2014, Cummings et al. 2018). Apart from the use of approved drugs, several clinical attempts have been made to treat AD progression by using various other strategies, such as immunotherapy against β-amyloid and beta-secretase (BACE) inhibitor administration, but the results have been disappointing (Cummings et al. 2018). These results show that addressing only the "β-amyloid cascade hypothesis" cannot fully control the progression of the disease, and this hypothesis also cannot explain the advanced neuronal damage in AD. Therefore, identifying new pharmacological targets for AD treatment is an active area of research.

In most neurodegenerative processes, including AD, neuroinflammation and oxidative stress (OS) are common traits. It is well-accepted that Ca^{2+} dysfunction is a consequence of homeostatic imbalance in nerve cells that unleashes a string of molecular and cellular processes, including neuroinflammation, OS, changes in neuronal plasticity, differential expression of glutamate and cholinergic receptors, and amyloid pathology (Sompol and Norris. 2018). Together, these processes end with cognitive decline and neurodegeneration. Calcineurin (CaN), also known as protein phosphatase 2B, is a Ca^{2+}-dependent Ser/Thr phosphatase that is highly abundant in the brain, appearing at high levels in neurons and low levels in glia in healthy adult animals (Kuno et al. 1992). CaN is related to long-term potentiation (LTP) and long-term depression (LTD), and dysregulation of CaN has been linked with cognitive loss in an AD mouse model (Baumgärtel & Mansuye. 2012; Reese LC and Taglialatela G. 2011). Of importance, CaN levels and signaling are increased in the cortex in AD patients (Wu et al. 2010) and in the contexts of other human neurodegenerative pathologies, including Parkinson's disease (PD) (Caraveo et al. 2014), Lewy body aggregation (Martin et al. 2012), and vascular pathology (Pleiss et al. 2016b). Moreover, CaN activity prevents fear memory formation in the amygdala by dephosphorylating and inhibiting downstream kinases, including AKT and extracellular signal–regulated kinase (ERK) (Lin et al. 2003). N-methyl-D-aspartate receptor (NMDAR)

(Wang et al. 2018; Mulkey et al. 1994) and glycogen synthase kinase 3β (GSK3β) (Watanabe et al. 2015) are some of the key actors in central nervous system function that are controlled by the phosphatase activity of CaN, which in turn is controlled by calcium calmodulin kinase II (CaMKII) and intracellular Ca^{2+} levels (Bezprozvanny and Hiersinger. 2013). Nuclear factor of activated T-cells (NFAT) consists of at least two different components, one with nuclear localization and one that is phosphorylated and localized in the cytoplasm (Horsley and Pavlath. 2002). Furthermore, recently, the CaN pathway has been observed to link astrocytic Ca^{2+} dysregulation to neuroinflammation, glutamate, β-amyloid accumulation and synaptotoxicity (Sompol and Norris. 2018).

Imidazoline 2 receptors (I_2-IRs) (Bousquet et al. 2020) are increased in AD brains (Ruiz J et al. 1993; García-Sevilla et al. 1998), and radioactive ligands have been studied as biomarkers for AD and PD progression in patients (Tyacke et al. 2018; Wilson et al. 2019). There is evidence that I_2-IR ligands reduce neurodegenerative processes, including cognitive decline, neuroinflammation, OS and AD hallmarks, but less is known about the upstream mechanism involved in the beneficial effects of I_2-IR modulation. Thus, the objective of this work was to delineate the molecular mechanisms involved in the neuroprotective effect of I_2-IR modulation in a mouse model of AD linked to the aging process, the senescence-accelerated mouse prone 8 (SAMP8) model. To this end, we used a newly synthesized I_2-IR ligand, diethyl (1RS,3aSR,6aSR)-5-(3-chloro-4-fluorophenyl)-4,6-dioxo-1-phenyl-1,3a,4,5,6,6a-hexahydropyrrolo[3,4-c]pyrrole-1-phosphonate, named B06, which has outstanding affinity and selectivity for I_2-IRs over α2 adrenoreceptors (Escolano et al. 2019).

The SAMP8 strain is a nontransgenic mouse strain established through phenotypic selection of the AKR/J mouse strain and is an attractive model with which to study aging processes, especially age-related deterioration of learning and memory, emotional disorders and neurochemical alterations (Takeda et al. 2009, Pallas. 2012). At approximately 5 months of age, the mice begin to undergo an accelerated process of senescence, and the brain aging manifests as severe cognitive decline and neuroinflammation (Akiguchi et al. 2017). It is considered a late-onset AD mouse model characterized by altered amyloid precursor protein (APP) processing and high levels of tau hyperphosphorylation (Canudas

et al. 2005; Morley et al., 2012). Moreover, inflammatory and OS markers are present at early ages and during adulthood (Griñán-Ferré et al. 2015, 2016).

2. Methods

2.1 *In vivo* studies in mice

Twelve-month-old female SAMP8 mice (n = 23) (Envigo, Sant Feliu de Codines,Barcelona, Spain)) were used to carry out cognitive and molecular analyses. The animals were randomly allocated into two experimental groups: the SAMP8 control group (control) (n=12), which was administered vehicle (2-hydroxypropyl)-β-cyclodextrin 1.8% in drinking water, and the SAMP8 group, which was treated with the I_2-IR ligand B06 (5 mg/kg) (n=11). The animals had free access to food and water and were kept under standard temperature conditions (22 ± 2°C) and 12-hour/12-hour light/dark cycles (300 lux/0 lux). B06 (5 mg/kg/day) was diluted in 1.8% (2-hydroxypropyl)-β-cyclodextrin and administered through drinking water. After 4 weeks of treatment, behavioral and cognitive tests, including short- and long-term memory, were performed to study the effects of treatment on learning and memory. Weight and water consumption were controlled each week, and the B06 concentration was adjusted accordingly to reach the optimal dose until euthanasia. The mice were euthanized 3 days after behavioral test completion by cervical dislocation. The brains were immediately removed from the skulls and frozen on powdered dry ice. The samples were stored at -80°C until the biochemical experiments.

The studies and procedures for the mouse behavior tests, brain dissection and extractions followed the ARRIVE and standard ethical guidelines (European Communities Council Directive 2010/63/EU and Guidelines for the Care and Use of Mammals in Neuroscience and Behavioral Research, National Research Council 2003) and were approved by Bioethical Committees from the University of Barcelona and the Government of Catalonia. All efforts were made to minimize the number of animals used and their suffering.

2.2 Novel object recognition test (NORT)

Briefly, mice were placed in a 90° two-arm 25-cm-long, 20-cm-high, 5-cm-wide black maze. Before performing the test, the mice were individually habituated to the apparatus for

10 minutes for 3 days. On day 4, the animals were allowed to freely explore in a 10-minute acquisition trial (first trial), for which they were placed in the maze in the presence of two identical objects at the end of each arm (Fig. 1A). After a delay (2 h for short-term memory evaluation and 24 h for long-term evaluation), the animal was allowed to explore the old object and one novel object in each trial (Fig. 1A). The time that the mice spent exploring the novel object (TN) and the time that the mice spent exploring the old object (TO) were measured. A DI was defined as (TN−TO)/(TN+TO). Exploration of an object was defined as pointing the nose towards the object at a distance ≤2 cm and/or touching it with the nose. Turning or sitting around the object was not considered exploration. To avoid object preference biases, the objects were counterbalanced.

2.3 Open field test (OFT)

The open field test (OFT) was performed as previously described (Griñán-Ferré et al., 2015) (Fig. 1B). Briefly, mice were placed at the center of and allowed to explore a white plywood box (50x50x25 cm) for 5 minutes. Behavior was scored with SMART® ver. 3.0 software, and each trial was recorded for later analysis. The parameters scored included the center stay duration, number of rearings, number of defecations, and distance traveled.

2.4 Determination of oxidative stress

Hydrogen peroxide (H_2O_2) was measured as an indicator of OS, and it was quantified using a hydrogen peroxide assay kit (Cat. No. MAK165, Sigma-Aldrich, Saint Louis, Missouri, Estats Units) according to the manufacturer's instructions.

2.5 Immunodetection experiments

2.5.1. Brain processing

Three days after the behavioral and cognitive tests, mice were euthanized for protein extraction and RNA and DNA isolation. After euthanasia, the brains were immediately removed from the skulls, and the hippocampi were dissected, frozen and maintained at -80°C.

For an IHC experiment, mice were anesthetized (ketamine 100 mg/kg and xylazine 10 mg/kg, intraperitoneally) and then perfused with 4% paraformaldehyde (PFA) diluted in 0.1 M phosphate buffer solution intracardially. Their brains were removed and postfixed in 4% PFA overnight at 4°C. Afterwards, the solutions were changed to PFA + 15% sucrose. Finally, the brains were frozen on powdered dry ice and stored at -80°C until sectioning.

2.5.2 Protein level determination by Western blotting

For subcellular fractionation, 150 µL of buffer A (10 mM HEPES pH 7.9, 10 mM KCl, 0.1 mM EDTA pH 8, 0.1 mM EGTA pH 8, 1 mM DTT, 1 mM PMSF, protease inhibitors) was added to each sample, and the mixtures were incubated on ice for 15 min. After this time, the samples were homogenized with a tissue homogenizer, 12.5 µL Igepal 1% was added, and the Eppendorf tubes were vortexed for 15 s. Following 30 s of full-speed centrifugation at 4°C, the supernatants (cytoplasmic fractions) were collected; 80 µL of buffer C (20 mM HEPES pH 7.9, 0,4 M NaCl, 1 mM EDTA pH 8, 0.1 mM EGTA pH 8, 20% glycerol 1 mM DTT, 1 mM PMSF, protease inhibitors) was added to each pellet, and the pellets were incubated under agitation at 4°C for 15 min. Subsequently, the samples were centrifuged for 10 min at full speed at 4°C. The supernatants (nuclear fractions) were collected.

For Western blotting (WB), aliquots of 20 µg of hippocampal protein were used. Protein samples from mice were separated by sodium dodecyl sulfate-polyacrylamide gel electrophoresis (SDS-PAGE) (8-12%) and transferred onto polyvinylidene difluoride (PVDF) membranes (Millipore). Afterwards, the membranes were blocked in 5% nonfat milk in 0.1% Tris-buffered saline with Tween 20 (TBS-T) for 1 hour at room temperature before being incubated overnight at 4°C with the primary antibodies listed in Table 1.

The membranes were washed and incubated with secondary antibodies for 1 hour at room temperature. Immunoreactive proteins were viewed with a chemiluminescence-based detection kit following the manufacturer's protocol (ECL Kit; Millipore, Burlington, Massachusetts, USA), and digital images were acquired using a ChemiDoc XRS+ System (Bio-Rad, Hercules, California, USA). Semiquantitative analyses were carried out using ImageLab software (Bio-Rad), and the results are expressed in arbitrary units (AU), with the control protein levels set as 100%. Protein loading was routinely monitored by immunodetection of glyceraldehyde-3-phosphate dehydrogenase (GAPDH) or β-actin.

2.5.3. Immunofluorescence

Brain coronal sections of 30 μm were obtained (Leica Microsystems CM 3050S cryostat, Wetzlar, Germany) and kept in a cryoprotectant solution at -20°C until use. Free-floating slices were placed in a 24-well plate and washed with 0.01 M PBS + 1% Triton X-100. Next, the free-floating sections were blocked with a solution containing 5% fetal bovine serum (FBS), 1% Triton X-100, 0.01 M PBS + gelatin 0.2% for 2 h at room temperature; washed with PBST (PBS 0.1 M, 1% Triton X-100) five times for 5 min each; and incubated with the primary antibodies listed in Table 2 overnight at 4°C. On the following day, the coronal slices were washed with PBST 6 times for 5 min each and then incubated with the secondary antibodies listed in Table 2 at room temperature for 2 h. Later, the sections were coincubated with 5 μM Hoechst staining solution (Sigma-Aldrich,) for 5 min in the dark at room temperature and washed with 0.01 M PBS. Finally, the slices were mounted using Fluoromount-G (EMS, Hatfield, Pennsylvania, USA), and image acquisition was performed with a fluorescence laser microscope (Olympus BX41, Hamburg, Germany) by using x4 and x10 magnification. At least four images from 4 different individuals in each group were analyzed with ImageJ/Fiji software available online from the National Institutes of Health.

2.6 RNA extraction and gene expression determination

Total RNA isolation was carried out using TRIzol® reagent according to the manufacturer's instructions. The yield, purity, and quality of RNA were determined spectrophotometrically with a NanoDrop™ ND-1000 apparatus (Thermo Scientific, Waltham, Massachusetts,USA) and an Agilent 2100B Bioanalyzer (Agilent Technologies, Santa Clara, California, USA). RNA samples with 260/280 ratios and RINs higher than 1.9 and 7.5, respectively, were selected. Reverse transcription-polymerase chain reaction (RT-PCR) was performed. Briefly, 2 μg of messenger RNA (mRNA) was reverse-transcribed using a high-capacity cDNA reverse transcription kit (Applied Biosystems, Foster City, California, USD).

SYBR® Green real-time PCR was performed on a StepOnePlus Detection System (Applied Biosystems) with SYBR® Green PCR master mix (Applied Biosystems). Each reaction

mixture contained 6.75 μL of complementary DNA (cDNA) (with a concentration of 2 μg), 0.75 μL of each primer (with a concentration of 100 nM), and 6.75 μL of SYBR® Green PCR master mix (2X).

TaqMan-based real-time PCR (Applied Biosystems) was also performed in a StepOnePlus Detection System (Applied Biosystems). Each 20 μL TaqMan reaction contained 9 μL of cDNA (25 ng), 1 μL of 20X TaqMan gene expression assay probe and 10 μL of 2X TaqMan universal PCR master mix.

The data were analyzed utilizing the comparative cycle threshold (Ct) (ΔΔCt) method, in which the levels of a housekeeping gene are used to normalize differences in sample loading and preparation. Normalization of expression levels was performed with *β-actin* for SYBR® Green-based real-time PCR and *Gapdh* for TaqMan-based real-time PCR. The primer sequences and TaqMan probes used in this study are presented in Table 3. Each sample was analyzed in duplicate, and the results represent the n-fold differences in the transcript levels among different groups.

2.7 Statistical analysis

Statistical analysis was conducted using GraphPad Prism ver. 8 statistical software. The data are expressed as the mean ± standard error of the mean (SEM). Means were compared with two-tailed Student's t-test. Statistical significance was considered when p values were <0.05. Statistical outliers were determined with Grubbs' test and when necessary were removed from the analyses.

3. Results

3.1 Prevention of memory loss and behavioral impairment in SAMP8 mice after I_2-IR ligand treatment

The NORT demonstrated significant differences between the control and I_2-IR ligand B06 groups in both short- and long-term evaluations. Significantly higher DI values were obtained for the B06-treated mice than for the control mice at 2 h and 24 h after novel object exposure, indicating a neuroprotective action of B06 against the characteristic SAMP8 mouse memory loss (Figs. 1C-D).

In addition, the results regarding locomotor activity, time spent in the center area and number of rearings, as assessed with the OFT paradigm, revealed significant changes in behavior in the B06 group in comparison with the control group (Figs. 1E-G).

3.2 AD hallmark modifications in the hippocampi of SAMP8 mice induced by I_2-IR ligand treatment

The levels of key proteins involved in APP processing were evaluated. The I_2-IR ligand B06 promoted significant increases in soluble APPα (sAPPα) levels but clearly tended to decrease soluble APPβ (sAPPβ) levels (Figs. 2A-B). Accordingly, the gene expression of *Adam10*, a constitutive α-secretase, increased, indicating a shift to the nonamyloidogenic pathway (Fig. 2C). Moreover, the gene expression of both *insulin-degrading enzyme* (*Ide*) and *neprilysin* (*Nep*) was increased after B06 treatment (Fig. 2C).

Tau hyperphosphorylation is a characteristic posttranslational modification in aged SAMP8 mice. B06 treatment induced significant decreases in phosphorylation at the Ser404 and Ser396 sites in tau protein (Figs. 3A-B). There are two main kinases implicated in tau hyperphosphorylation: glycogen synthase kinase 3β (GSK3β) and cyclin-dependent kinase 5 (CDK5). GSK3β phosphorylated at Ser9 is the inactive form of the enzyme and is correlated with reduced tau phosphorylation. As expected, the I_2-IR ligand B06 increased p-GSK3β (Ser9) levels, indicating that it reduced kinase activity (Fig. 3C). CDK5 is also activated by phosphorylation, and p25, a coactivator, controls its activity. The results showed that the I2-IR ligand-treated group presented decreases in the p-CDK5 level and p25/p35 ratio (Figs. 3D-E).

3.3 I_2-IR ligand treatment changes synaptic and apoptotic markers in SAMP8 mice

The I_2-IR ligand B06 reduced the protein levels of the NMDA 2B receptor, increased those of the form phosphorylated at Tyr1472 and increased those of the NMDA 2A receptor significantly (Figs. 4A-C).

The levels of calcium/calmodulin-dependent protein kinase II (CaMKII), a marker of synaptic plasticity, did not show significant changes, but the levels of the phosphorylated form of cAMP response element-binding protein (CREB) were dramatically increased (Fig.

4D) in the B06 group. Accordingly, the gene expression of the CREB target *brain-derived neurotrophic factor (Bdnf)* was increased in the B06 group (Fig. 4G).

Protein kinase A (PKA) is a master regulator of the activity of CREB, among other transcription factors. B06-treated animals showed increased protein levels of PKA a (the catalytic fragment) (Fig. 4E). We found significant recovery of AKT, also known as protein kinase B, phosphorylation and subsequent activation (Fig. 4F) in the B06 group, indicating a pathway of neuroprotective regulation after B06 treatment.

B-cell lymphoma 2 (BCL-2), Bax, BCL-2-associated agonist of cell death (BAD) and Caspase 3 are key factors in apoptotic signaling in neurons. B06 was able to reduce Caspase 3 and Bcl-2-like protein 4 (Bax) protein levels; surprisingly, it also reduced BCL-2 protein levels (Figs. 5A-C). An increase in p-BAD was also observed (Fig. 5D); however, in this case, phosphorylation of BAD indicated a lack of capacity to form apoptotic pores by dimerizing BAD, which subsequently weakened the proapoptotic role of this factor. Overall, prevention of apoptotic mechanisms followed treatment with the I_2-IR ligand B06.

3.4 Neuroinflammation and oxidative state changes in SAMP8 mice after I_2-IR ligand treatment

GFAP protein levels were highly significantly decreased in the B06 group (Fig. 6A), indicating that astrogliosis and neuroinflammation processes were ameliorated in I_2-IR ligand B06-treated mice. Astrocytes control glutamatergic signaling through glutamate transporters, and B06 was able to enhance the protein levels of excitatory amino acid transporter (EAAT) 2 (Fig. 6B). The expression of proinflammatory cytokines, such as *interleukin (Il)-6, Il-18, Il-1β, interferon (Ifn)γ, tumor necrosis factor-alpha (Tnf-α),* and *C-X-C motif chemokine ligand 10 (Cxcl-10),* was decreased after treatment with the I_2-IR ligand B06 (Fig. 6C), and the decrease reached significance for *Il-6, Il-18 and Il-1β.* H_2O_2 levels in the hippocampus were significantly diminished in the B06 mouse group, showing that global redox homeostasis was shifted due to the antioxidant role of the I_2-IR ligand in SAMP8 mice (Fig. 6D). The expression of *nuclear factor-erythroid 2-related factor 1 (Nrf1),* a key gene controlling the oxidative cell environment, was higher in the group treated with the I_2-IR ligand B06 than in the untreated mouse group (Fig. 6E). In addition, the gene expression of antioxidant machinery enzymes such as *hemoxygenase 1 (Hmox 1)*

was increased, whereas that of *aldehyde dehydrogenase 2 (Aldh2)* was reduced, indicating that B06 prevented SAMP8 brain from experiencing an oxidant environment by neutralizing radical oxygen species (ROS) (Fig. 6E). Conversely, a significant increase in the gene expression of *inducible nitric oxide synthase (iNOS)* was found, although this increase could have improved synaptic function (Fig. 6E). Finally, immunostaining quantification of GFAP fluorescence intensity demonstrated that B06 treatment significantly reduced GFAP staining, especially in the dentate gyrus (DG) and CA1 regions (Figs. 6F-M), suggesting a reduction in astrogliosis. Moreover, immunostaining quantification of S100A9 fluorescence intensity showed that B06 treatment reduced S100A9 staining, especially in the CA1 and CA3 regions, but the reductions were not significant (Figs. 6F-M).

3.5 I_2-IR ligand treatment modifies CaN/NFAT signaling in the SAMP8 mouse hippocampus

In light of the obtained results, we focused on CaN, an upstream protein with phosphatase activity toward CREB or BAD that plays a role in neurodegeneration. The protein levels of CaN A, the active form, were reduced after treatment with the I_2-IR ligand B06 (Fig. 7A). We also evaluated $NFAT_{C1}$, a different target of CaN. The results showed an increase in the phosphorylated form (Fig. 7B).

As a summary of the results, Figure 8 shows the molecular alterations related to cognitive improvement as well as the key role of CaN in controlling the cellular response after treatment with the I_2-IR ligand B06.

4 Discussion

Here, we report that treatment with the I_2-IR ligand B06 in the SAMP8 mouse model, a model of neurodegeneration linked to aging that is considered to recapitulate late-onset AD, has beneficial effects via modulation of the CaN pathway. Imidazoline receptors were described in the nineties, and I_2-IRs are related to neurodegenerative diseases such as AD (García-Sevilla et al. 1998), Huntington's disease (Reynolds et al. 1996) and PD (Reynolds et al. 1996; Tyacke et al. 2018; Wilson et al. 2019). However, the signal transduction

pathway for I_2-IR remains elusive (Bousquet et al, 2020). Previous reports have indicated putative roles related to monoamine oxidase (MAO) A or B (McDonald et al. 2010) and intracellular calcium concentration control through NMDA receptors or intracellular calcium stores (Jiang et al. 2010; Zhao Han et al. 2013). Recently, we have demonstrated that ligands for I_2-IRs are able to prevent neurodegeneration by acting on the apoptotic mechanism (Abas et al. 2017), and decreasing the activity of kinases (CDK5, GSK3β, etc.) (Abas et al. 2016, Griñán-Ferré et al. 2019), leading to the recovery of cognitive capabilities in an AD mouse model (Griñán-Ferré et al. 2019). However, the intrinsic mechanisms that induce these changes are not precisely known.

B06 is a new improved I_2-IR ligand with a lower Ki for I_2-IR than previous ligands and high selectivity for I_2-IRs over α_2 adrenoceptors (Escolano et al. 2019). The latter characteristic is of the utmost importance for avoidance of undesirable adverse effects on, for example, the vascular system. We have previously reported that administration of B06 to the 5xFAD mouse model, a transgenic representative model of AD, reduces cognitive decline, neuroinflammation, tau hyperphosphorylation and APP processing (Escolano et al. 2019).

In the present work, we demonstrated that the I_2-IR ligand B06 was able to improve cognition and ameliorate anxiety-like behavior in aged SAMP8 mice. Furthermore, we confirmed that on the molecular level, treatment with B06 reduced the exhibition of AD hallmarks, such as APP processing and tau hyperphosphorylation; inhibited tau kinase (CDK5 and GSK3β) activation; reduced the gene expression of neuroinflammation markers, such as *Il-6, Il-18,* and *Tnf-α*; and decreased OS.

When the apoptotic pathway was studied, decreases in Caspase 3, Bax, and BCL-2 levels were found. However, there has been a lack of consistency among I_2-IR studies regarding the reduction in apoptotic signaling (Garau et al. 2013). Our results are consistent with those of several studies showing that administration of I_2-IR ligands such as 2-BFI and BU224 can reduce apoptotic marker levels in the rat brain cortex (Li. 2017). Considering that I_2-IRs have been reported to be involved in key pathways associated with neurodegeneration, we also evaluated several master pathways in B06-treated senescent

mice, including those that are under the control of cytosolic calcium, astrocyte activation and synaptic neural plasticity. The localization of I_2-IRs remains elusive, but several studies have reported astrocytes as a major cell type with I_2-IR binding sites (Choi et al. 2018). Of note, astrogliosis and activated microglial cells are associated with amyloid processing, indicating that this AD hallmark is a major trigger of gliosis (Vehmas et al. 2003). After B06 treatment, a very significant decrease in the expression of the hippocampal panastrocytic reactive marker GFAP indicated strong control of neuroinflammation and a reduction in astrogliosis that in turn could prevent neuronal function loss. Moreover, S100A9, a Ca^{2+}-binding protein with a critical role in modulating the inflammatory response and inducing cytokine release by astrocytes (Wang et al. 2018), was used as a marker of neuroinflammation mediated by reactive astrocytes. In our study, we found clear reductions in two hippocampal areas, CA1 and CA3, confirming a reduction in the inflammatory state after treatment with B06. Likewise, the expression of the EAAT2 isoform (or Glt 1), a glutamate transporter predominantly located in astrocytes, was increased after treatment with the I_2-IR ligand B06. EAAT2 is implicated in glutamate clearance and has a leading role in the removal of excess glutamate and other potentially toxic mediators (Furman and Norris. 2014). In line with these findings, our previous results for two other I_2-IR ligands (Griñán-Ferré et al. 2018) showed the same action regarding astrogliosis. However, in contrast, another study on the I_2-IR ligand LSL60101 showed induction of reactive astrocytosis in the facial motor nuclei of neonate rats after short-term treatment (Casanovas et al. 2000), suggesting that the effects differ depending on both the physicochemical properties of the I_2-IR ligand and the experimental model.

Notably, in astrocytes, increased CaN activity can lead to modification of the kinase activity of GSK3β (Watanabe et al. 2015). Calcium entry through NMDA2B receptors enhances the activation of GSK3β through CaN phosphatase activity, and in turn, GSK3β amplifies this phosphatase activity, dephosphorylating CREB (Szatmari et al. 2005; Wang et al. 2018). In addition, the interaction of I_2-IR ligands with NMDA receptors has been well described (Olmos, De-Gregorio-Rocasolano, et al. 1999; Olmos, Ribera & Garcia-Sevilla. 1996). Thus, our results support the idea that modulation of I_2-IRs by B06 is able to induce changes in NMDA receptors. We definitively observed changes in NMDA receptor

subunit composition and activation. On the one hand, increases in NMDA2A receptor protein levels were observed. On the other hand, decreases in NMDA2B receptor protein levels with increased phosphorylation were observed. These changes are associated with LTP, which may partially explain the improvement in cognition observed in B06-treated SAMP8 mice.

To further elucidate the molecular mechanisms modulated by B06, we examined the negative crosstalk between AKT and GSK3β signaling that participates in synaptic plasticity (Bradley et al. 2012) controlled by CaN phosphatase activity. As mentioned, B06 treatment reduced GSK3β activation by increasing the levels of its inactive form phosphorylated at Ser9, whereas it activated AKT signaling. Because AKT is a recognized prosurvival molecule that participates in neural plasticity, modulation of AKT signaling in animals treated with the I_2-IR ligand B06 likely contributed to the favorable effects on cognition observed in SAMP8 mice (Zhu et al. 2001; Sun and Nan. 2017).

p-CREB controls the expression of genes related to synaptic disruption and LTP, such as *Bdnf* (Bridi et al. 2017). Neuronal growth and survival require the expression of CREB target genes that control various proteins, including BDNF and its receptor tropomyosin-related kinase B (TrkB) (Zhang et al. 2012). On the one hand, treatment with the I_2-IR ligand B06 increased nuclear p-CREB levels and increased *Bdnf* gene expression. On the other hand, B06 increased the levels of PKA, which can drive p-CREB nuclear translocation. Of note, PKA acts as a negative modulator of $NFATc_1$, a transcription factor that regulates the transcription of genes that play crucial roles in axonal outgrowth control (Sheridan et al. 2002). Interestingly, I_2-IR ligand treatment induced an increase in $NFATc_1$ phosphorylation in parallel with decreases in *Il-6, Ifn-γ* and *Tnf-α* gene expression. $NFATc_1$ and CaN are master regulators that control EAAT2 up- or downregulation (Su et al. 2003). We hypothesize that the observed changes in $NFATc_1$ are responsible for the increase in EAAT2 described above.

$NFATc_1$ is dephosphorylated by CaN, which enables its nuclear translocation. Continuous NFAT activation and nuclear signaling result in neurodegenerative morphological

abnormalities, including neuritic dystrophy, dendritic spine loss and modulation of β-amyloid accumulation. Indeed, NFAT activity stimulates the amyloidogenic pathway (Jin et al. 2012; Sompol et al. 2017), and its inhibition has been found to significantly reduce β-amyloid plaque formation in an AD mouse model (Furman et al. 2012). Therefore, a reduction in nuclear NFAT should have beneficial effects in senescence models, in which overactivation of neurodegenerative pathways is a key cause of cognitive decline (Griñán-Ferré et al. 2015, 2016).

The last finding, closely linked with the findings described above, is the implication of CaN in the beneficial effects of the I_2-IR ligand B06 in SAMP8 mice. CaN is a multicomponent protein in which CaN A has phosphatase activity regulated by calcium levels (Rusnak F et al. 2010). Calcium dysregulation can be induced by age-related changes, such as OS and inflammation (Furman et al. 2014; Reese and Taglialatela. 2014). Furthermore, inhibition of CaN signaling produces neuroprotection in models of injury and disease (O'Donell et al. 2016; Xiong et al. 2018), reduces neuroinflammation (Furman and Norris, 2014) and cognitive impairment (Liu et al. 2018), and improves synapse function (Kim et al. 2015). Consistent with these findings, we hypothesized that in SAMP8 mice, which are characterized by neuroinflammation and OS, an imbalance of calcium levels occurs, activating CaN A and inducing neurodegeneration. Specifically, astrocytic CaN is activated under inflammatory conditions and can, for example, activate GSK3β and inactivate AKT, influencing NMDAR-mediated axonal outgrowth (Wang et al. 2018). As stated above, the I_2-IR ligand B06 reduced CaN A protein levels, and accordingly, we found activation of AKT and strong inactivation of GSK3β.

Regarding the OS observations, CaN can be activated after H_2O_2 addition to neuronal cultures (Sée and Loeffler. 2001). Likewise, the reductions in OS markers after treatment with the I_2-IR ligand B06 could have also contributed to a reduction in CaN activity. These findings correlate with cognitive improvement, increasing neuroprotective signaling and reducing tau hyperphosphorylation. Conversely, CaN A can dephosphorylate tau. However, the balance between tau phosphorylation and dephosphorylation is due to a shift in tau kinase activity (Yu et al. 2008). Hyperactivation of the PP1A domain of CaN A results in

dephosphorylation of a few transcription factors, such as CREB (which blocks CREB translocation to the nucleus) and NFAT (which enables NFAT translocation to the nucleus). In both cases, the reduced synaptic and growth gene transcription necessitates plasticity, and the increases in the expression of proinflammatory factors participate in neurodegenerative processes. Moreover, hyperactivation of the phosphatase 2B (PP2B) domain increases BAD dephosphorylation, favoring the action of BAD as a proapoptotic factor (Mukherjee et al. 2010).

In conclusion, the data from our study demonstrate that modulation of I_2-IRs by B06 reduces neuroinflammation, OS and CaN protein levels in SAMP8 mice. The decreases in CaN protein levels can explain the changes in CREB, $NFAT_{c1}$ and BAD phosphorylation levels. In addition, the decreases in CaN levels result in modification of the kinase activity of GSK3β and AKT, among other molecules, leading to reduced tau hyperphosphorylation and preventing cognitive decline in SAMP8 mice. Collectively, our findings provide evidence that the CaN pathway is a critical component of the neuroprotective effects of I_2-IR ligands on SAMP8 model mice, providing insight into several molecular modifications observed after I_2-IR ligand treatment. In the future, a deeper knowledge of the role of the I_2-IR signaling cascade in AD will provide new therapeutic targets for cognitive decline and AD.

Declarations

Not applicable

Competing interest statement

Authors have no competing interests to declare

Author Contributions

CGF, MP and CE contributed to conceptualization and funding acquisition. SA, SRA and AB synthetized and purified B06. CGF and FV realized experiments and data formal analysis. CGF, CE, FV and MP wrote-reviewed and edited the manuscript. All authors read and approved the final version of the manuscript.

References

1. Abás S, Erdozain AM, Keller B, Rodríguez-Arévalo S, Callado LF, García-Sevilla JA, Escolano C. Neuroprotective effects of a structurally new family of high affinity imidazoline I2 receptors ligands. ACS Chem. Neurosci. 2017;8(4):737-742. doi: 10.1021/acschemneuro.6b00426.

2. Abás S, Estarellas C, Luque FJ, Escolano C. 2015. Easy access to (2-imidazolin-4-yl)phosphonates by a microwave assisted multicomponent reaction. Tetrahedron 2015;71:2872-2881. https://doi.org/10.1016/j.tet.2015.03.065.

3. Akiguchi I, Pallàs M, Budka H, Akiyama H, Ueno M, Han J, Yagi H, Nishikawa T, Chiba Y, Sugiyama H, Takahashi R, Unno K, Higuchi K, Hosokawa M. SAMP8 mice as a neuropathological model of accelerated brain aging and dementia: Toshio Takeda's legacy and future directions. Neuropathology. 2017;37:293-305. doi: 10.1111/neup.12373.

4. Antunes M, Biala G. The novel object recognition memory: neuro- biology, test procedure, and its modifications. Cogn. Process. 2012;13:93-110. doi: 10.1007/s10339-011-0430-z.

5. Baumgärtel, K. & Mansuy, I. M., 2012. Neural functions of CaN in synaptic plasticity and memory. Learn. Mem. Cold Spring Harb. 2012;19:375–384. doi: 10.1101/lm.027201.112.

6. Bezprozvanny I, Hiesinger PR. The synaptic maintenance problem: membrane recycling, Ca2+ homeostasis and late onset degeneration. Mol Neurodegener. 2013; 8:23 doi: 10.1186/1750-1326-8-23.

7. Boersma MCH, Dresselhaus EC, De Biase LM, Mihalas AB, Bergles DE, Meffert MK. A Requirement for Nuclear Factor-□B in Developmental and Plasticity-Associated Synaptogenesis. J. Neurosc. 2011;31(14):5414-5425. DOI: 10.1523/JNEUROSCI.2456-10.2011.

8. Bon C, Bohme GA, Doble A, Stutzmann JM, Blanchard JC. A role for nitric oxide in long-term potentiation. Eur J Neurosci. 1991;4:420–424. doi: 10.1111/j.1460-9568.1992.tb00891.x.

9. Bousquet, P, Hudson, A, García-Sevilla, JA, Li, JX. Imidazoline receptors system: the past, the present and the future. Pharmacol. Rev. 2020; 72:1-30. Doi: 10.1124/pr.118.016311.

10. Bradley CA, Peineau S, Taghibiglou C, Nicolas CS, Whitcomb DG, Bortolotto ZA, Kaang BK, Cho K, Wang YT, Collingridge GL. A pivotal role of GSK3 in synaptic plasticity. Front Mol Neurosci. 2012; 5:13 doi: 10.3389/fnmol.2012.00013.

11. Bridi MS, Hawk JD, Chatterjee S, Safe S, Abel T. Pharmacological Activators of the NR4A Nuclear Receptors Enhance LTP in a CREB/CBP-Dependent Manner. Neuropsychopharmacology. 2017;42(6):1243-1253. doi: 10.1038/npp.2016.253.

12. Canudas AM, Gutierrez-Cuesta J, Rodríguez MI, Acuña-Castroviejo D, Sureda FX, Camins A, Pallàs M. Hyperphosphorylation of microtubule-associated protein tau in senescence-accelerated mouse (SAM). Mech Ageing Dev. 2005;126(12): 1300-4.

13. Caraveo G, Auluck PK, Whitesell L, Chung CY, Baru V, Mosharov E. V, Yan X, Ben-Johny M, Soste M, Picotti P, Kim H, Caldwell KA, Caldwell GA, Sulzer D, Yue DT, Lindquist S. Calcineurin determines toxic versus beneficial responses to alpha-synuclein. Proc. Natl. Acad. Sci. USA 111, 2014;111(34):E3544-E3552.doi:10.1073/pnas.1413201111.

14. Casanovas A, Olmos G, Ribera J, Boronat MA, Esquerda JE, García-Sevilla JA. Induction of reactive astrocytosis and prevention of motoneuron cell death by the I(2)-imidazoline receptor ligand LSL 60101. Br J Pharmacol. 2000;130(8):1767-1776. doi:10.1038/sj.bjp.0703485.

15. Choi DH, Yun JH, Lee J. Protective effect of the imidazoline I2 receptor agonist 2-BFI on oxidative cytotoxicity in astrocytes. Biochem Biophys Res Commun. 2018;503(4):3011-3016. https://doi.org/10.1016/j.bbrc.2018.08.086.

16. Cummings J, Lee G, Ritter A, Zhong K. Alzheimer's disease drug development pipeline: 2018. Alzheimers Dement (NY). 2018;4:195–214 doi: 10.1016/j.trci.2018.03.009.

17. Cummings J. Lessons learned from Alzheimer Disease: Clinical Trials with negative outcomes. Clin Transl Sci. 2018;11:147-152 doi:10.1111/cts.12491.

18. Cummings JL, Morstorf T, Zhong K. Alzheimer's disease drug-development pipeline: few candidates, frequent failures. Alzheimers Res Ther 2014;6(4):37. doi: 10.1186/alzrt269.

19. Escolano C, Pallás M, Griñán-Ferré C, Abás S, Callado LF, García-Sevilla JA. Synthetic I2 imidazoline receptor ligands for prevention or treatment of human brain disorders. WO 2019/121853 A1, June 2019.

20. Furman JL, Norris CM. Calcineurin and glial signaling: neuroinflammation and beyond. J Neuroinflammation. 2014;11:158. doi: 10.1186/s12974-014-0158-7.

21. Furman JL, Sama DM, Gant JC, Beckett TL, Murphy MP, Bachstetter AD, Van Eldik LJ, Norris CM. Targeting astrocytes ameliorates neu- rologic changes in a mouse model of Alzheimer's disease. J Neurosci 2012; 32:16129 –16140.

22. García-Sevilla JA, Escribá PV, Walzer C, Bouras C, Guimón J. Imidazoline receptor proteins in brains of patients with Alzheimer's disease. Neurosci Lett. 1998;247: 95-98.

23. Garau C, Miralles A, Garcia-Sevilla JA. Chronic treatment with selective I2-imidazoline receptor ligands decreases the content of pro-apoptotic markers in rat brain. J Psychopharmacol. 2013;27(2):123–134. doi: 10.1177/0269881112450785.

24. GBD 2016 Neurology Collaborators. Global, regional, and national burden of neurological disorders, 1990-2016: a systematic analysis for the Global Burden of Disease Study 2016. 2010. Lancet Neurol. 18(5):459-480. doi: 10.1016/S1474-4422(18)30499-X.

25. Griñán-Ferré C, Palomera-Avalos V, Puigoriol-Illamola D, Camins A, Porquet D, Plà V, Aguado F, Pallàs M. Behaviour and cognitive changes correlated with hippocampal neuroinflammaging and neuronal markers in SAMP8, a model of accelerated senescence. Exp Gerontol. 2016;80:57-69. https://doi.org/10.1016/j.exger.2016.03.014.

26. Griñan-Ferré C, Puigoriol-Illamola D, Palomera-Ávalos V. Environmental enrichment modified epigenetic mechanisms in SAMP8 mouse hippocampus by reducing oxidative stress and inflammaging and achievingneuroprotection. Front. Aging Neurosci. 2016; 8: 1-12.

27. Griñán-Ferré C, Vasilopoulou F, Abàs S, Rodríguez-Arévalo S, Bagán A, Sureda FX, Pérez B, Callado LF, García-Sevilla JA, García-Fuster MJ, Escolano C, Pallàs M. Behavioral and cognitive improvement induced by novel imidazoline I2 receptor ligands in female SAMP8 mice. Neurotherapeutics. 2019;16:416-431. https://doi.org/10.1007/s13311-018-00681-5.

28. Hopp SC, Bihlmeyer NA, Corradi JP, Vanderburg C, Cacace AM, Das S, Clark TW, Betensky RA, Hyman BT, Hudry E. Neuronal calcineurin transcriptional targets parallel changes observed in Alzheimer disease brain. J Neurochem. 2018;147(1): 24-39. doi: 10.1111/jnc.14469.

29. Horsley V, Pavlath GK. NFAT ubiquitous regulator of cell differentiation and adaptation. J Cell Biol. 2002;156(5):771-774 doi: 10.1083/jcb.200111073.

30. Jin SM1, Cho HJ, Kim YW, Hwang JY, Mook-Jung I. Aβ-induced Ca(2+) influx regulates astrocytic BACE1 expression via calcineurin/NFAT4 signals. Biochem Biophys Res Commun. 2012;425(3):649-655 doi: 10.1016/j.bbrc.2012.07.123.

31. Jiang SX, Zheng RY, Zeng JQ, Li XL, Han Z, Hou ST. Reversible inhibition of intracellular calcium influx through NMDA receptors by imidazoline I(2) receptor antegonists. Eur J Pharmacol. 2010;629 (1-3): 12-9. doi:10.1016/j.ejphar.2009.11.063.

32. Kim S, Violette CJ, Ziff EB. Reduction of increased calcineurin activity rescues impaired homeostatic synaptic plasticity in presenilin 1 M146V mutant. Neurobiol Aging. 2015; 36(12): 3239–3246.doi: 10.1016/j.neurobiolaging.2015.09.007.

33. Kipanyula MJ, Kimaro WH, Seke Etet PF. The Emerging Roles of the Calcineurin-Nuclear Factor of Activated T-Lymphocytes Pathway in Nervous System Functions and Diseases. J Aging Res. 2016; 2016:5081021. doi: 10.1155/2016/5081021.

34. Kuno T, Mukai H, Ito A, Chang CD, Kishima K, Saito N, Tanaka C.Distinct cellular expression of calcineurin A alpha and A beta in rat brain. J Neurochem. 1992;58:1643–1651. 10.1111/j.1471-4159.1992.tb10036.x.

35. Li JX. Imidazoline I2 receptors: An update. Pharmacol Ther. 2017 Oct;178:48-56. doi: 10.1016/j.pharmthera.2017.03.009. Epub 2017 Mar 16. PMID: 28322973; PMCID: PMC5600648.

36. Lin CH, Lee CC & Gean PW. Involvement of a CaN cascade in amygdala depotentiation and quenching of fear memory. Mol Pharmacol. 2003;63:44–52. doi: https://doi.org/10.1124/mol.63.1.44.

37. Liu J, Si Z, Li S, Huang Z, He Y, Zhang T, Wang A. Prevents Cognitive Impairment by Inhibiting Reactive Astrogliosis in Pilocarpine-Induced Status Epilepticus Rats. Front Cell Neurosci. 2018;11:428. doi: 10.3389/fncel.2017.00428.

38. Martin ZS, Neugebauer V, Dineley KT, Kayed R, Zhang W, Reese LC, Taglialatela G. α-Synuclein oligomers oppose long-term potentiation and impair memory through a calcineurin-dependent mechanism: relevance to human synucleopathic diseases. J Neurochem. 2012;120(3):440-452. doi: 10.1111/j.1471-4159.2011.07576.x.

39. Martina L, Latypova X, Wilsona CM, Magnaudeix A, Perrin ML, Terro F. Tau protein phosphatases in Alzheimer's disease: The leading role of PP2A. Ageing Res Rev. 2003;12: 39–49.

40. McDonald GR, Olivieri A, Ramsat RR, Holt A. On the formation and nature of the imidazoline I2 binding site on human monoamine oxidase-B. Pharmacolo. Res.2010;62(6): 475-488 https://doi.org/10.1016/j.phrs.2010.09.001.

41. Morley JE, Farr SA, Kumar VB, Armbrecht HJ. The SAMP8 mouse: a model to develop therapeutic interventions for Alzheimer's disease. Curr. Pharm. Des. 2012; 18:1123-1130. 10.2174/138161212799315795.

42. Mukherjee A, Morales-Scheihing D, Gonzalez-Romero D, Green K, Taglialatela G, Soto C. CaN inhibition at the clinical phase of prion disease reduces neurodegeneration, improves behavioral alterations and increases animal survival. PLoS Pathog. 2010;6(10): e1001138 https://doi.org/10.1371/journal.ppat.1001138.

43. Mulkey RM, Endo S, Shenolikar S, Malenka RC. Involvement of a calcineurin/inhibitor-1 phosphatase cascade in hippocampal long-term depression. Nature. 1994;369(6480): 486-8.

44. O'Donnell JC, Jackson JG, Robinson MB. Transient oxygen/glucose deprivation causes a delayed loss of mitochondria and increases spontaneous calcium signaling in astrocytic processes. J. Neurosci. 2016;36, 7109–7127. doi: 10.1523/JNEUROSCI.4518-15.2016.

45. Olmos G, DeGregorio-Rocasolano N, Paz Regalado M, Gasull T, Assumpcio Boronat M, Trullas R, Garcia-Sevilla JA. Protection by imidazol(ine) drugs and agmatine of glutamate-induced neurotoxicity in cultured cerebellar granule cells through blockade of NMDA receptor. Br J Pharmacol. 1999;127(6):1317–1326. doi: 10.1038/sj.bjp.0702679.

46. Olmos G, Ribera J, Garcia-Sevilla JA. Imidazoli(di)ne compounds interact with the phencyclidine site of NMDA receptors in the rat brain. Eur J Pharmacol. 1996;310(2–3):273–276.

47. Pallàs M. Senescence-accelerated mice P8: a tool to study brain aging and Alzheimer's disease in a mouse model. ISRN Cell Biol. 2012; 2012:1-12. 10.5402/2012/917167.

48. Papa M, Pellicano MP, Sadile AG. Nitric oxide and long-term habituation to novelty in the rat. Ann NY Acad Sci. 1994;738:316–324.

49. Pleiss MM, Sompol P, Kraner SD, Mohmmad Abdul H, Furman JL, Guttmann RP, Wilcock DM, Nelson PT, Norris CM. Calcineurin proteolysis in astrocytes: Implications for impaired synaptic function. Biochim Biophys Acta. 2016;1862(9):1521-1532. doi: 10.1016/j.bbadis.2016.05.007.

50. Reese LC and Taglialatela G. A role of Calcineurin in Alzheimer's disease. Current Neuropharmacology. 2011;9(4):685-692 doi: 10.2174/157015911798376316.

51. Reynolds GP, Boulton RM, Pearson SJ, Hudson AL, Nutt DJ. Imidazoline binding sites in Huntington's and Parkinson's disease putamen. Eur J Pharmacol. 1996;301(1-3):R19-21

52. Ruiz J, Martin I, Callado LF, Meana JJ, Barturen F, Garca-Sevilla JA. Non-adrenoreceptor [3H]idazoxan binding sites (I2-imidazoline sites) are increased in postmoterm brain from patients with Alzheimer's disease. Neuroscience letters. 1993;160:109-112. https://doi.org/10.1016/0304-3940(93)90925-B.

53. Rusnak F, Mertz P. Calcineurin: form and function. Physiol Rev. 2000;80(4):1483-521.

54. Sée V, Loeffler JP. Oxidative stress induces neuronal death by recruiting a protease and phosphatase-gated mechanism. J Biol Chem. 2001;276(37):35049-59. doi: 10.1074/jbc.M104988200.

55. Serrano-Pozo A, Frosch MP, Masliah E, Hyman BT. Neuropathological alterations in Alzheimer disease. Cold Spring Harb Perspect Med. 2011. Sep;1(1):a006189. doi: 10.1101/cshperspect.a006189. PMID: 22229116; PMCID: PMC3234452.

56. Sheridan CM, Heist EK, Beals CR, Crabtree GR, Gardner P, 2002 Protein kinase A negatively modulates the nuclear accumulation of NF-ATc1 by priming for subsequent phosphorylation by glycogen synthase kinase-3. J Biol Chem. 2002; 277(50): 48664-76. doi: 10.1074/jbc.M20702920.

57. Sompol P and Norris C. Ca2+, astrocyte activation and calcineurin/NFAT signaling in age-related neurodegenerative diseases. Front Aging Neurosci. 2018;10:199. doi: 10.3389/fnagi.2018.00199.

58. Su ZZ, Leszczyniecka M, Kang DC, Sarkar D, Chao W, Volsky DJ, Fisher PB. Insights into glutamate transport regulation in human astrocytes: cloning of the promoter for excitatory amino acid transporter 2 (EAAT2).Proc Natl Acad Sci U S A. 2003;100:1955–196 doi: 10.1073/pnas.0136555100.

59. Sun J, Nan G. The extracellular signal-regulated kinase 1/2 pathway in neurological diseases: A potential therapeutic target (Review) Int J Mol Med. 2017;39(6):1338–1346. doi: 10.3892/ijmm.2017.2962.

60. Szatmari E, Habas A, Yang P, Zheng JJ, Hagg T, Hetman M. A positive feedback loop between glycogen synthase kinase 3beta and protein phosphatase 1 after stimulation of NR2B NMDA receptors in forebrain neurons. J Biol Chem. 2004;280(45):37526-35. doi: 10.1074/jbc.M502699200.

61. Takeda T. Senescence-accelerated mouse (SAM) with special references to neurodegeneration models, SAMP8 and SAMP10 mice. Neurochem Res. 2009;34:639-659. doi: 10.1007/s11064-009-9922-y.

62. Tyacke RJ, Myers JFM, Venkataraman A, Mick I, Turton S, Passchier J, Husbands SM, Rabiner EA, Gunn RN, Murphy PS, Parker CA, Nutt DJ. Evaluation of 11C-BU99008, a PET Ligand for the Imidazoline2 Binding Site in Human Brain. J Nucl Med. 2018;59(10):1597-1602. doi: 10.2967/jnumed.118.208009.

63. Vehmas AK, Kawas CH, Stewart WF, Troncoso JC. Immune reactive cells in senile plaques and cognitive decline in Alzheimer's disease. Neurobiol Aging. 2003;24(2):321-331. doi:10.1016/s0197-4580(02)00090-8.

64. Wang XS, Chen YY, Shang XF, Zhu ZG, Chen GQ, Han Z, Shao B, Yang HM, Xu HQ, Chen JF, Zheng RY. Idazoxan attenuates spinal cord injury by enhanced astrocytic activation and reduced microglial activation in rat experimental autoimmune encephalomyelitis. Brain Res. 2009;1253:198-209. https://doi.org/10.1016/j.brainres.2008.11.059.

65. Wang Y, Tang JL, Xu X, Zhou XP, Du J, Wang X, Zhou Y, Zhu Q, Yao LL, Wang YG, Hou S, Huang Z. NMDA receptors inhibit axonal outgrowth by inactivating AKT and

activating GSK-3β via calcineurin in cultured immature hippocampal neurons. Exp Cell Res. 2018; 371(2):389-398. doi: 10.1016/j.yexcr.2018.08.033.

66. Watanabe K, Uemura K, Asada M, Masato M, Akiyama H, Shinohama S, Takahashi R, Kinoshita A. The participation of insuline-like growth factor- binding protein 3 released by astrocytes in the pathology of Alzheimer's disease. Molecular Brain. 2015;8:82. doi: 10.1186/s13041-015-0174-2.

67. Wilson H, Dervenoulas G, Pagano G, Tyacke RJ, Polychronis S, Myers J, Gunn RN, Rabiner EA, Nutt D, Politis M. Imidazoline 2 binding sites reflecting astroglia pathology in Parkinson's disease: an in vivo11C-BU99008 PET study. Brain, 2019;142(10):3116–3128. https://doi.org/10.1093/brain/awz260.

68. Wu HY, Hudry E, Hashimoto T, Kuchibhotla K, Rozkalne A, Fan Z, Spires-Jones T, Xie H, Arbel-Ornath M, Grosskreutz CL, Bacskai BJ, Hyman BT. Amyloid beta induces the morphological neurodegenerative triad of spine loss, dendritic simplification, and neuritic dystrophies through calcineurin activation. J Neurosci. 2010;30(7):2636-49. doi: 10.1523/JNEUROSCI.4456-0.

69. Xiong TQ, Chen LM, Tan BH, Guo CY, Li YN, Zhang YF, Li SL, Zhao H, Li YC. The effects of calcineurin inhibitor FK506 on actin cytoskeleton, neuronal survival and glial reactions after pilocarpine-induced status epilepticus in mice. Epilepsy Res. 2918;140:138–147. doi: 10.1016/j.eplepsyres.2018.01.007.

70. Yu D, Tong L, Song G, Lin W, Zhang L, Bai W, Gong H, Yin Y, Wei Q. Tau binds both subunits of CaN, and binding is impaired by calmodulin. Biochim Biophy Acta. 2008;1783, 2255–2261 https://doi.org/10.1016/j.bbamcr.2008.06.015.

71. Zhang F, Kang Z, Li W, Xiao Z, Zhou X. Roles of brain-derived neurotrophic factor/tropomyosin-related kinase B (BDNF/TrkB) signalling in Alzheimer's disease. J Clin Neurosci. 2012;19(7):946-949. doi:10.1016/j.jocn.2011.12.022.

72. Zhao H, Jin-Long Y, Susan XJ, Sheng-Tao H, Rong-Yuan Z. Fast, Non-Competitive and Reversible inhibition of NMDA-Activated Currents by 2-BFI confers Neuroprotection. PloS One.2013; 8(5):e64894. doi: 10.1371/journal.pone.0064894.

73. Zhu D, Liu SH, Sun HS, Lu YM. Expression of Inducible Nitric Oxide Synthase after Focal Cerebral Ischemia Stimulates Neurogenesis in the Adult Rodent Dentate Gyrus. J Neurosci. 2003;23(1):223–229. https://doi.org/10.1523/JNEUROSCI.23-01-00223.2003.

74. Zhu X, Castellani RJ, Takeda A, Nunomura A, Atwood CS, Perry G, Smith MA. Differential activation of neuronal ERK, JNK/SAPK and p38 in Alzheimer disease: the 'two hit' hypothesis. Mech Ageing Dev. 2001;123:39–46. doi: 10.1016/S0047-6374(01)00342-6.

Figure legends

Figure 1. Scheme for NORT (A) and OFT (B) experimental paradigms. The I2-IR ligand improved the novel object recognition abilities (measured as Discrimination Index, DI) in SAMP8 treated with B06 at 5 mg/Kg/day (B06 5mg/kg) in comparison with the SAMP8 Control both in summary short-term memory (C) and summary long-term memory (D). In the Open Field Test (OFT) 12-month-old SAMP8 treated with B06 at 5 mg/Kg/day (B06 5mg/kg) presented a significant increase in the distance traveled (E), the percentage of time spent in Center zone (F) and the number of Rearings (G). Values represented are mean ± Standard error of the mean (SEM); n = 15 (Control n = 8, B06 n = 7); *p<0.05; **p<0.01; ***p<0.001; ****p<0.0001 vs. Control.

Figure 2. Treatment with the I2-IR ligand B06 resulted in significant differences in the amyloid processing and Aβ degradation pathway between the 12-month-old control SAMP8 (Control) and the SAMP8 treated with B06 at 5 mg/Kg/day (B06 5mg/kg). Representative western blot for sAPPα and sAPPβ protein levels and quantification (A, B). Values in bar graphs were adjusted to 100% for the protein of control SAMP8 (Control). Representative gene expression for Adam10, Ide and Nep (C). Gene expression levels were determined by real-time PCR. Values are the mean ± Standard error of the mean (SEM); (n= 3-5 animals per group); *p<0.05; **p<0.01 vs. Control.

Figure 3. The I2-IR treatment mediated a significant decrease in Tau phosphorylation and the implicated kinases in 12-month-old SAMP8 treated with B06 at 5 mg/Kg/day (B06 5mg/kg) when compared to control SAMP8 (Control). Representative western blot for ratio p-Tau (Ser396 and Ser404), Ratio p-GSK3β (Ser9), Ratio p-CDK5, p25/35 and quantification (A-E). Values in bar graphs were adjusted to 100% for protein of control

SAMP8 (Control). Values are the mean ± Standard error of the mean (SEM); (n= 3-5 animals per group); *p<0.05; **p<0.01; ***p<0.001; ****p<0.0001 vs. Control.

Figure 4. Changes in NMDARs, neuronal plasticity and Kinase pathways induced by I2-IR ligand B06 in 12-month-old SAMP8 after treatment at 5 mg/Kg/day (B06 5mg/kg) in comparison with 12-month-old control SAMP8 (Control). Representative western blot for NMDAR2B, NMDAR2A, Ratio p-NMDAR2B (Tyr1472). Ratio p-CREB in nucleus protein levels and quantification (A-D). Representative Western blot for kinases PKA, Ratio p-AKT and quantification (E, F). Values in bar graphs were adjusted to 100% for the protein of control SAMP8 (Control). Representative gene expression for Bdnf (G). Gene expression levels were determined by real-time PCR. Values are the mean ± Standard error of the mean (SEM); (n= 3-5 animals per group); *p<0.05; **p<0.01; ***p<0.001 vs. Control.

Figure 5. Treatment with the I2-IR ligand B06 suppressed apoptosis by inhibiting the implicated apoptotic factors in 12-month-old SAMP8 treated with B06 at 5 mg/Kg/day (B06 5mg/kg) as compared to control SAMP8 (Control). Representative western blot for caspase-3, Bax, BCL-2, Ratio p-BAD (Ser136) and quantification (A-D). Values in bar graphs were adjusted to 100% for the protein of control SAMP8 (Control). Values are the mean ± Standard error of the mean (SEM); (n= 3-5 animals per group); *p<0.05; **p<0.01 vs. Control.

Figure 6. I2-IR ligand, B06, attenuated neuroinflammation and OS state in 12-month-old SAMP8 treated mice at 5 mg/Kg/day (B06 5mg/kg) when compared to the control SAMP8 (Control). Representative western blot for GFAP, GLT-1/EAAT-2 (A-B). Representative gene expression for inflammatory markers such as Il-6, Il-18 Il-1β, Ifn-γ, Tnf-α and Cxcl-10 (C) and OS markers such as Hmox1, iNOS, Nrf1 and Aldh2 (E). Quantification of Intracellular H202 (μM) (D). Gene expression levels were determined by real-time PCR. Values in bar graphs were adjusted to 100% for the protein of control SAMP8 (Control). Representative images for GFAP (F) and S100A9 immunostaining (F) and quantifications for GFAP and S100A9 on the bar chart (G-M). DG: Dentate Gyrus. Scale bar for

immunohistochemical images is 200 μm. Values are the mean ± Standard error of the mean (SEM); (n= 3-5 animals per group); *p<0.05; ***p<0.001 vs. Control.

Figure 7. Modulation of CaN signaling after B06 treatment in 12-month-old SAMP8 treated mice at 5 mg/Kg/day (B06 5mg/kg). Representative western blot for CaN A, ratio p-NFATc1/NFATc1 and quantification (A, B). Values in bar graphs were adjusted to 100% for protein of control SAMP8 (Control). Values are the mean ± Standard error of the mean (SEM); (n= 3-5 animals per group); *p<0.05; **p<0.01 vs. Control.

Figure 8. Graphical Abstract showing molecular changes in CaN signaling after treatment with B06.

Figure 1

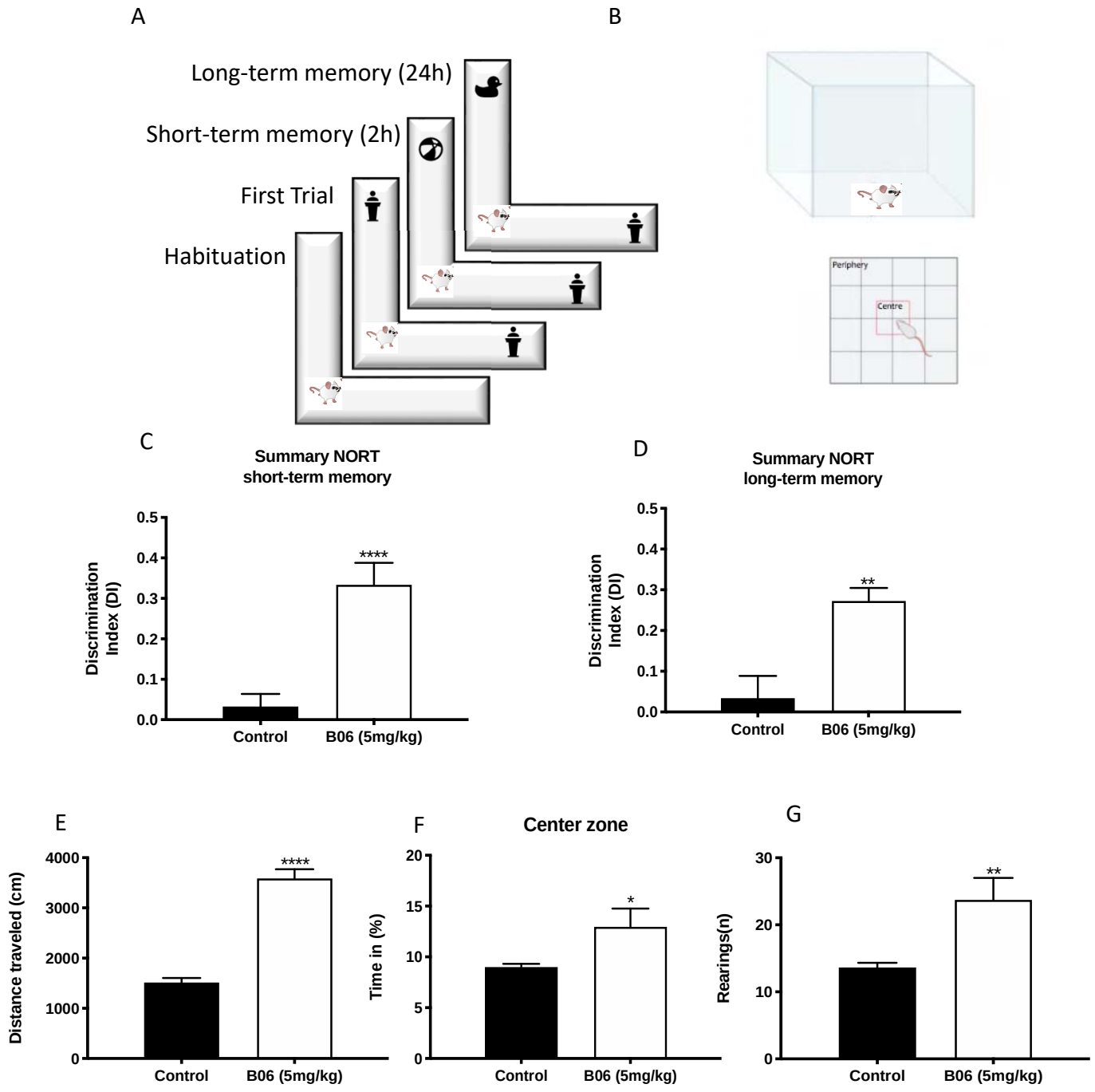

Figure 2

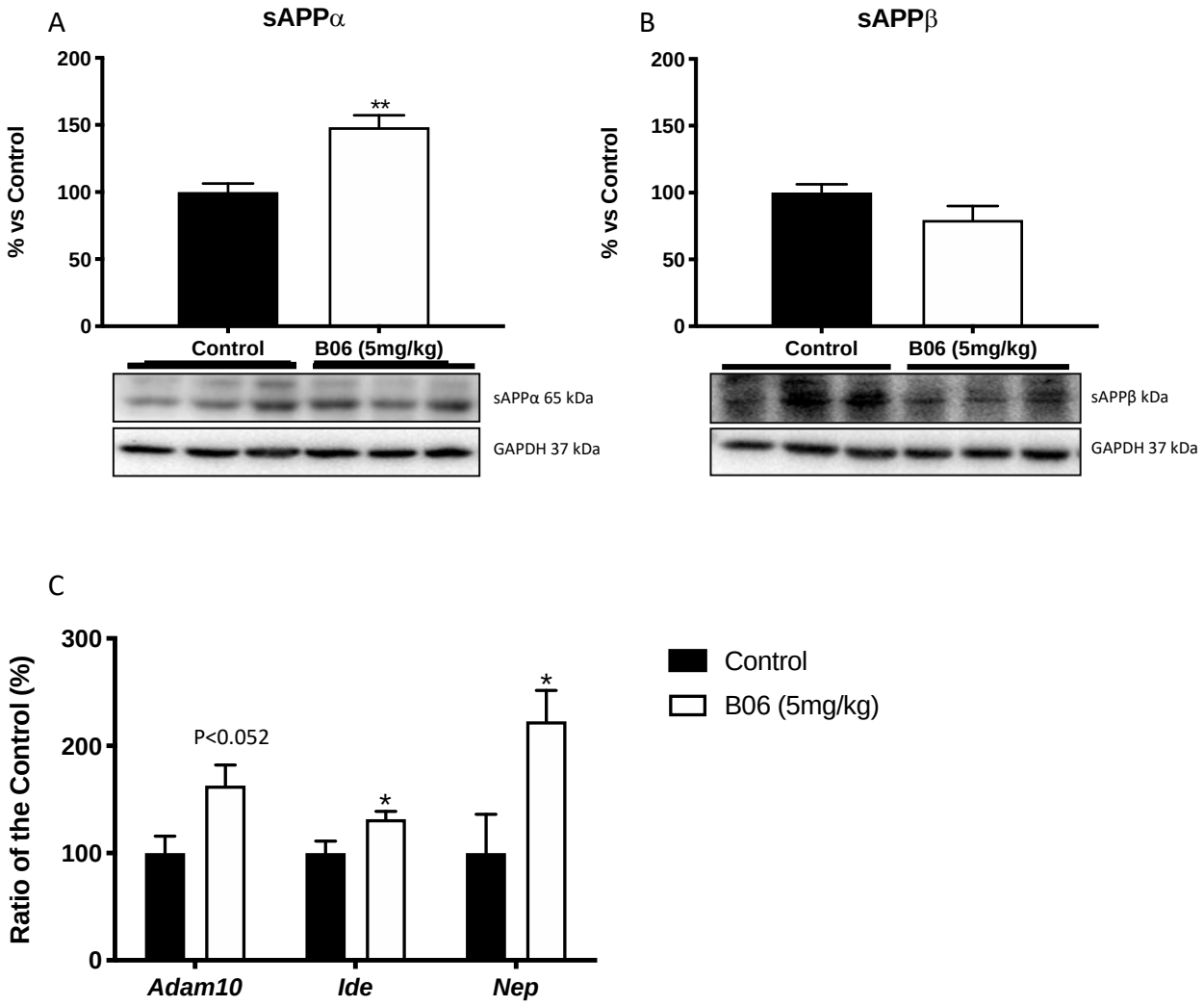
A
sAPPα
% vs Control
200
150
100
50
0
**
Control
B06 (5mg/kg)
sAPPα 65 kDa
GAPDH 37 kDa
B
sAPPβ
% vs Control
200
150
100
50
0
Control
B06 (5mg/kg)
sAPPβ kDa
GAPDH 37 kDa
C
Ratio of the Control (%)
300
200
100
0
P<0.052
*
*
Adam10
Ide
Nep
Control
B06 (5mg/kg)

line figure 3
Figure 3

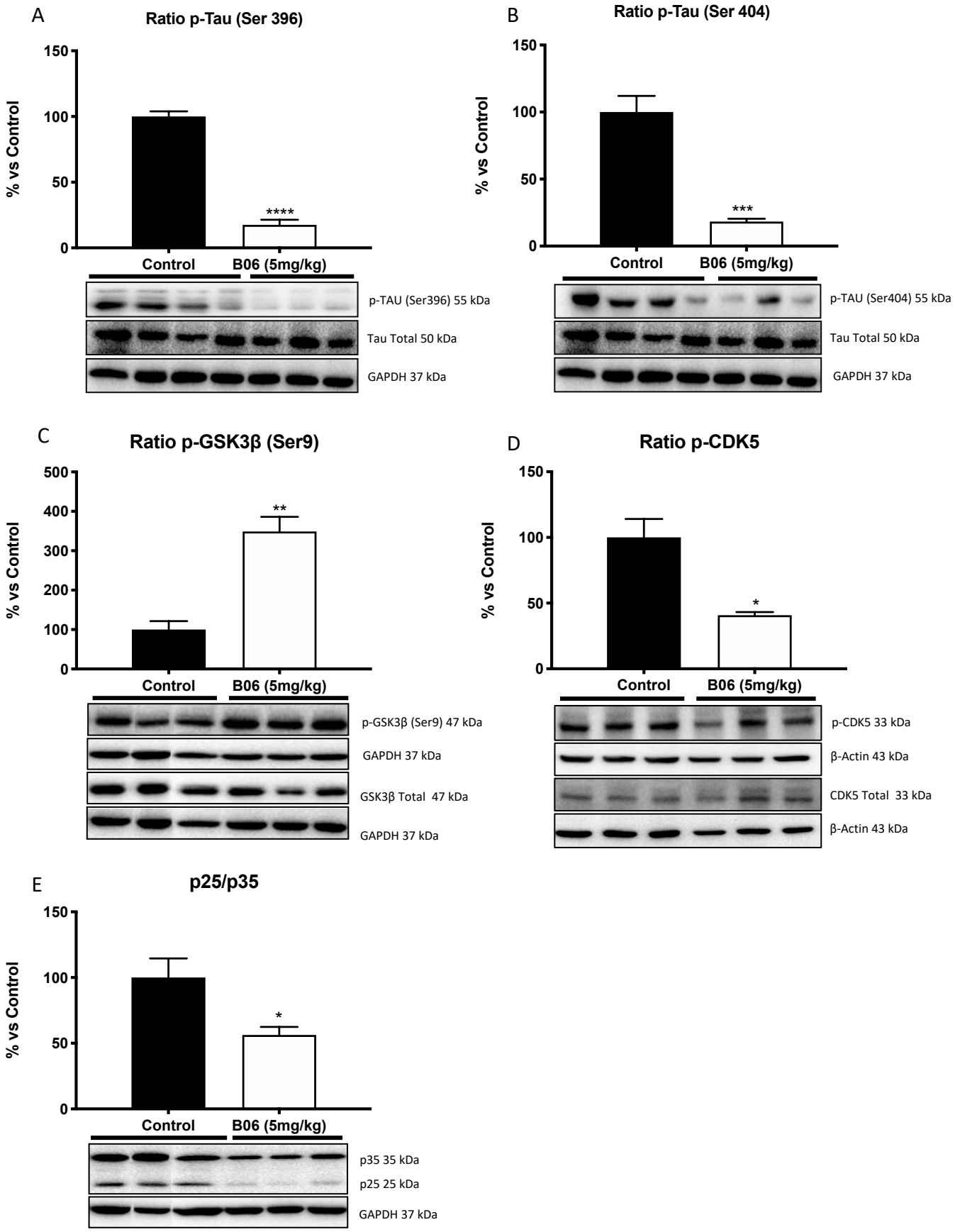

line figure 4

Figure 4

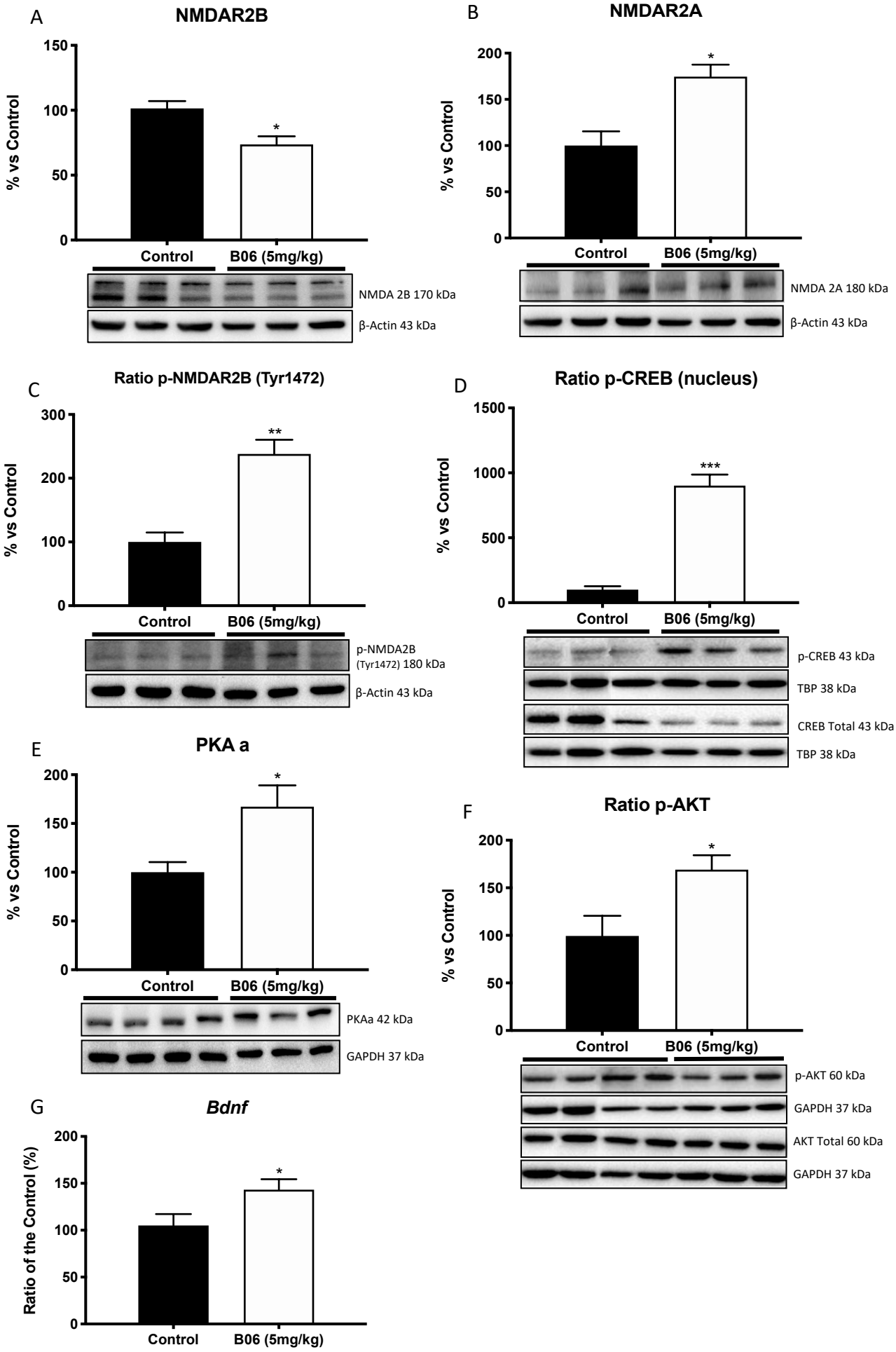

line figure 5

Click here to access/download;line figure;Figure 5_j.pdf

Figure 5

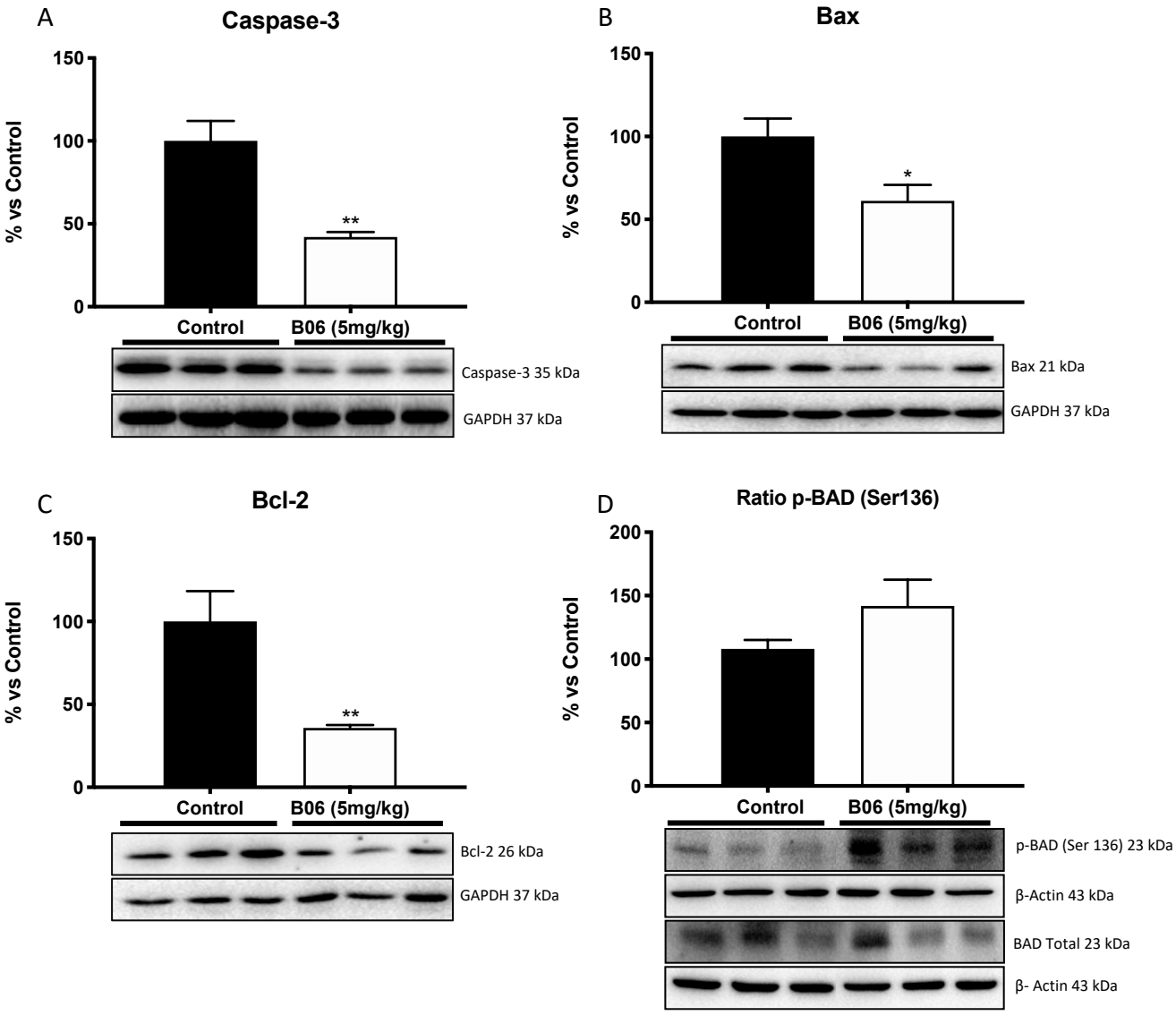

Figure 6

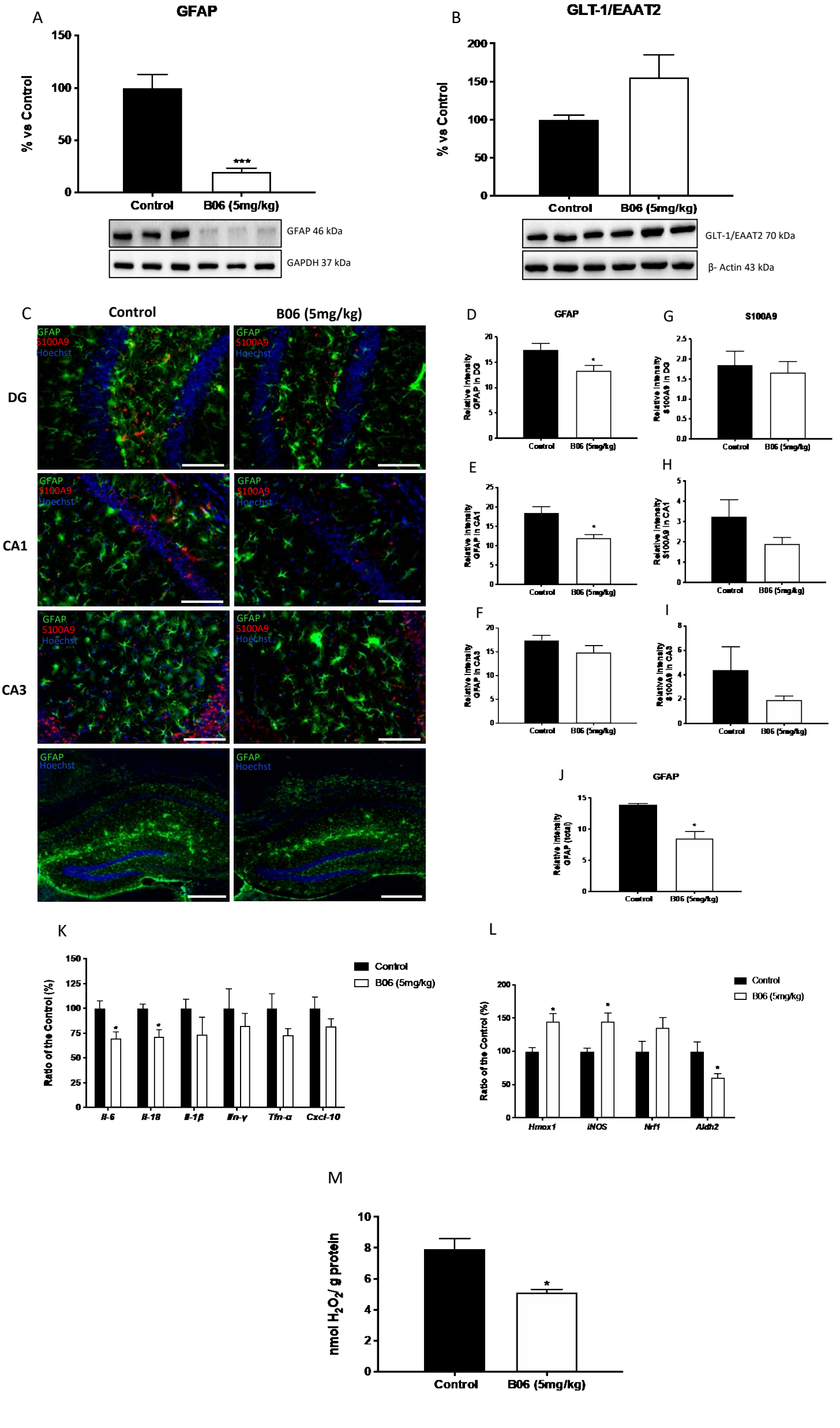

line figure 7

Click here to access/download;line figure;Figure 7_j.pdf

Figure 7

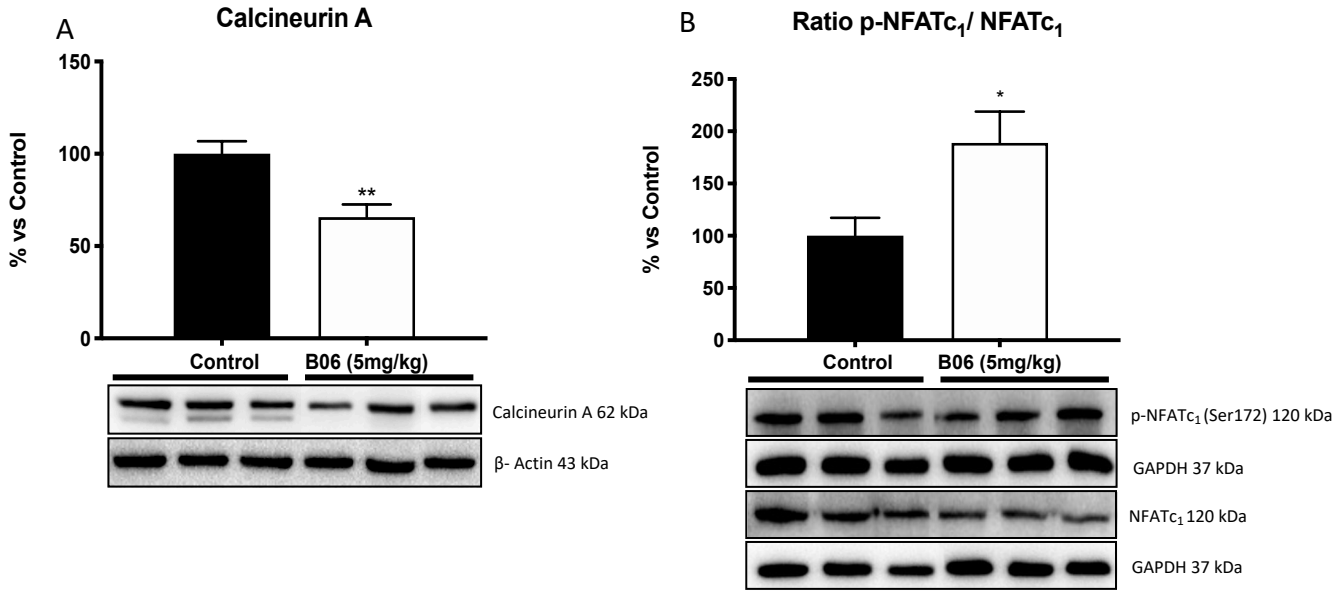

colour figure
Figure 8

Click here to access/download;colour figure;Figure 8_abstractGraph V2.pdf

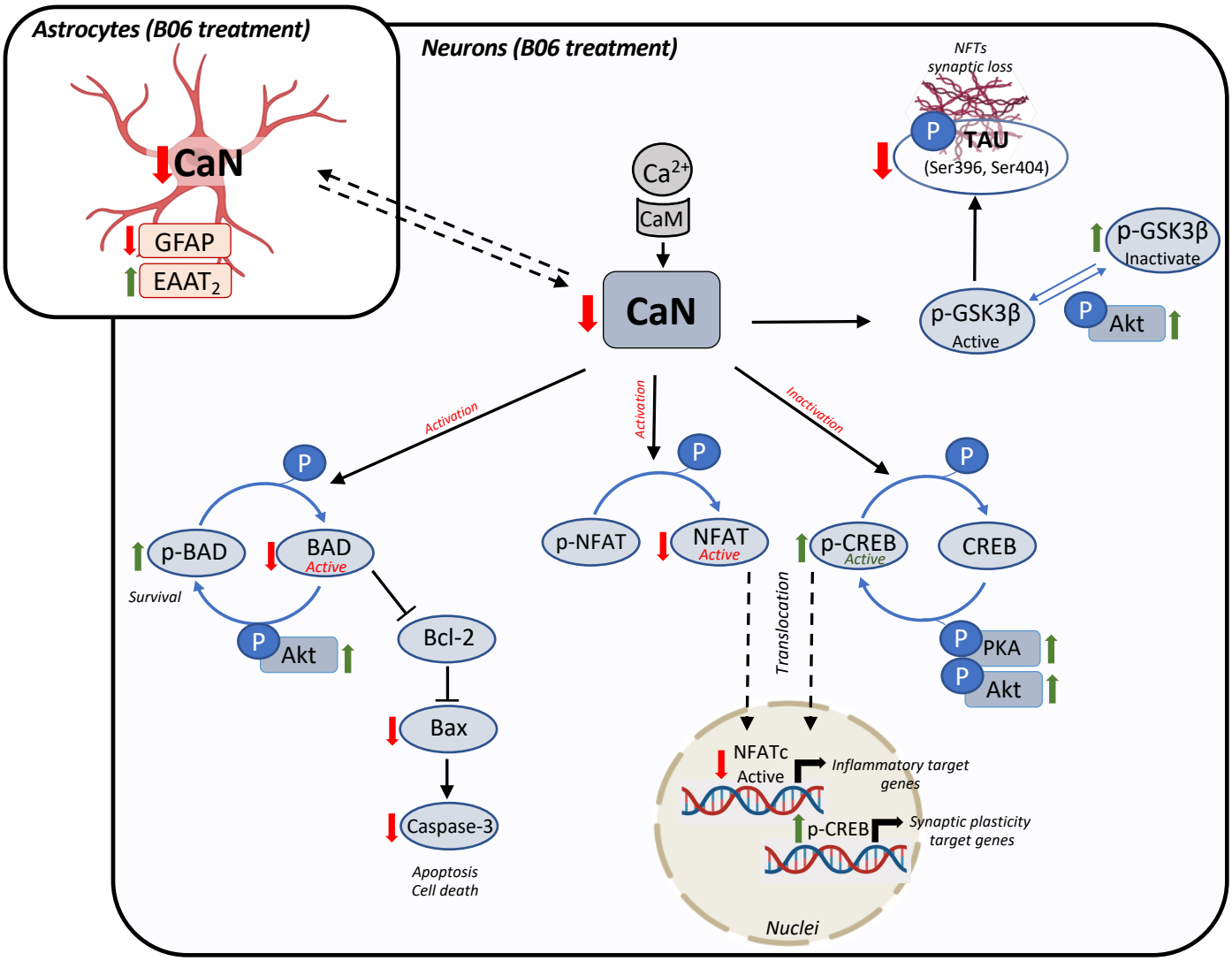

Table 1. Antibodies used in Western blot studies.

Antibody	Host	Source/Catalog	WB dilution
AKT	Rabbit	Cell Signaling/#9272	1:1000
Bad	Mouse	Santa Cruz/sc-8044	1:1000
Bax	Rabbit	Cell signaling/#2772	1:1000
Bcl-2	Rabbit	Cell Signaling/#2870	1:1000
Calcineurin A	Rabbit	BioRad/VPA00329	1:1000
Calpain	Mouse	BioRad/AHP2443	1:1000
CaMKII	Rabbit	Abcam/ab52476	1:1000
Caspase-3	Rabbit	Cell Signaling/#9662	1:1000
Cdk5	Rabbit	Santa Cruz/sc-173	1:1000
CREB (48H2)	Rabbit	Cell Signaling/#9197	1:1000
EAAT2	Mouse	Santa Cruz/sc-365634	1:1000
GFAP	Rabbit	Gene Tex/GTX100850	1:1000
GSK-3β	Rabbit	Cell Signaling/#9315S	1:1000
NFATc1	Rabbit	St John's/STJ24751	1:1000
NMDA2A	Mouse	Santa Cruz/sc-515148	1:1000
NMDA2B	Mouse	Santa Cruz/sc-365597	1:1000
P35/p25	Rabbit	Cell Signaling/#C64B10	1:1000
pAKT (Ser473)	Rabbit	Cell Signaling/#4060	1:1000
pBAD (Ser136)	Rabbit	Cell Signaling/#4366S	1:500
pCaMKII (Thr286)	Rabbit	SAB/#11287	1:1000
pCdk5 (Y15)	Rabbit	Abcam/ab63550	1:1000
pCREB (Ser133)	Rabbit	Cell Signaling/#9198	1:1000
P-p44/42 (T202/Y204)	Rabbit	Cell Signaling/#9101	1:1000
p-GSK-3beta	Rabbit	Cell Signaling/#9336	1:1000
PKA	Mouse	Santa Cruz/sc-28315	1:1000
p-NFAT (Ser172)	Rabbit	Invitrogen/PA5-64696	1:500
pNMDAR2B (Tyr1472)	Rabbit	Invitrogen/OPA1-04116	1:1000
p-Tau Ser396	Rabbit	Invitrogen/44-752G	1:1000
p-Tau Ser404	Rabbit	Invitrogen/44-758G	1:1000
sAPPα	Rabbit	Covance/SIG-39139-005	1:2000
sAPPβ	Rabbit	Covance/SIG-39138-05	1:2000
Tau total	Mouse	Invitrogen/AHB0042	1:1000

TBP	Mouse	Abcam/ab51841	1:1000
Actin	Mouse	Invitrogen/MA5-15739	1:2000
GAPDH	Mouse	Millipore/MAB374	1:5000
Goat-anti-mouse HRP conjugated		Biorad/170-5047	1:2000
Goat-anti-rabbit HRP conjugated		Biorad/170-6515	1:2000

Table 2. Reagents used in IHC studies.

Antibody	Host	Source/Catalog	IHC dilution
GFAP	Rabbit	DAKO/Z0334	1:400
S100A9	Mouse	R&D Systems/AF2065	1:400
Alexa Fluor 594 Goat anti-mouse IgM		Invitrogen/A21044	1:1000
Alexa Fluor 488 Rabbit anti-goat IgG		Invitrogen/A11078	1:400
Hoechst 33258 solution		Sigma-Aldrich/94403	

Table 3. Primers and probes used in qPCR studies.

SYBR Green primers

Target	Product size (bp)	Forward primer (5'-3')	Reverse primer (5'-3')
Ide	128	GCAACACCATACCCTGCTCT	TCCACATAAGCAAACGGGCT
Adam10	125	GGGAAGAAATGCAAGCTGAA	CTGTACAGCAGGGTCCTTGAC
Cxcl10	72	GGCTAGTCCTAATTGCCCTTGG	TTGTCTCAGGACCATGGCTTG
Il-6	189	ATCCAGTTGCCTTCTTGGGACTGA	TAAGCCTCCGACTTGTGAAGTGGT
Il-18	151	GTTTACAAGCATCCAGGCACAG	GAAGGTTTGAGGCGGCTTTC
Il-1β	179	TGTGAAATGCCACCTTTTGA	GGTCAAAGGTTTGGAAGCAG
Ifn-γ	87	CCTTCTTCAGCAACAGCAAGGCG	CTTGGCGCTGGACCTGTGGG
Tnf-α	157	TCGGGGTGATCGGTCCCCAA	TGGTTTGCTACGACGTGGGCT
iNOS	125	GGCAGCCTGAGAGACCTTTG	GGAAGCGTTTCGGGATCTGAA
Nrf1	114	AGCACGGAGTGACCCAAAC	TGTACGTGGCTACATGGACCT
Aldh2	189	GCAGGCGTACACAGAAGTGA	TGAGCTTCATCCCCTACCCA
Nep	196	TTGGGAGACCTGGCGGAAAC	CATTCCTTGGACCCTCACCCC
β-actin	190	CAACGAGCGGTTCCGAT	GCCACAGGTTCCATACCCA

Taqman probes

Target	Product size (bp)	Reference
Hmox1	69	Mm00516005_m1
Bdnf	71	Mm01334042_m1
Gapdh	109	Mm99999915_g1